Investigating the impact of HVAC and Sanitizer system design on the transmission of SARS-CoV-2 in Hospital Isolation Units

Investigating the impact of HVAC and Sanitizer system design on the transmission of SARS-CoV-2 in Hospital Isolation Units.

Narjisse Amahjour[a,b,*], Anas Sofi[b], Tariq Kamal[c], Abderrahman El Kharrim[b]

[a]*Instituto de Ciencias Matemáticas, CSIC, C/ Nicolás Cabrera 15, Campus Cantoblanco, Madrid, 28049, Spain*
[b]*Team: Energy, Materials and Numerical physics, Ecole Normale Supérieure, Abdelmalek Essaadi University, Tetouan, 93100, Morocco*
[c]*School of Technology and Innovations, University of Vaasa, Vaasa, FI-65101, Finland*

Abstract

The COVID-19 pandemic has presented unprecedented challenges to healthcare facilities worldwide. Hospital isolation units have played a crucial role in the management of COVID-19 patients. However, the transmission of the virus within these units can lead to severe consequences for patients, healthcare workers, and the broader community. This research proposes a framework to evaluate the impact of HVAC (Heating, Ventilation, and Air Conditioning) and sanitizer system design on the transmission of SARS-CoV-2 in isolation unit at Saniat Rmel Hospital in Tetouan Morocco by using computational fluid dynamics (CFD) and the realizable $k-\epsilon$ turbulence model. Furthermore, the study investigates the effect of different inlet air velocities on the dispersion of airborne viral particles in the isolation unit. The results indicate that the air change rate plays a critical role in the spread and concentration of pathogens in the isolation unit. It was determined that the high inlet air velocity can lead the particles fluid including the virus reaches the exhaust port in a short time, in addition, it can facilitate the distribution of sanitizer throughout an isolation unit, which could potentially reduce the concentration of the virus. The outcome suggests that the placement and orientation of the air conditioner combined with the sanitizer system have a significant impact on the movement characteristics of fluid particles within the enclosed environment.

Keywords: Computational fluid dynamics, Virus, isolation room, HVAC, sanitizer machine, air velocity

Nomenclature

Abbreviations

CFD Computational Fluid Dynamics

DRW Random Walk Model

FEM Finite Element Method

*narjisse.amahjour@gm.uca.es

HAVC	Heat Air Ventilation Conditioning
PTM	Particle Tracing Model
RANS	Reynolds averaged Navier-Stokes

Greek symbols

δ_{i_j}	Kronecker term
κ	Von Karman's constant
μ	dynamic viscosity ($Pa.s$)
μ	particle density (kg/m^3)
μ_t	turbulent dynamic viscosity($Pa.s$)
$\overline{\Omega_{i_j}}$	Average rate of the rotation tensor
ρ	fluid density (kg/m^3)
ρ	turbulent dissipation energy (m^2/s^2)
τ_p	particle velocity response time
τ_{i_j}	shear stress (N/m^2)
ξ	Vector of uncorrelated Gaussian random numbers
$C_\mu, C_{\epsilon 1}, C_{\epsilon 2}, \sigma_\epsilon, \sigma_k$	closure constants
tau_p	particle velocity response time

Parameters

ω	angular velocity (rad/s)
ω_i	mass fraction (m/s)
C_p	fluid heat capacity (J/K)
d_p	particle diameter (μ_m)
D_t	turbulence thermal diffusion (m^2/S)
F_a	additional external forces (N)
F_D	drag force (N)
F_g	gravity force (N)
F_t	total forces (N)
g	acceleration gravity (m/s^2)
j_i	diffusive mass flux of species

k	turbulent kinetic energy (m^2/s^2)
m_p	mass of the particle (kg)
p	pressure (Pa)
Q	heat source (J)
q	heat flux (W/m^2)
R_i	source term of species
S_{c_i}	turbulent Schmidt number
T	temperature(C)
T^+	dimensionless temperature
T_w	wall temperature(C)
$u_i'u_j'$	fluctuating velocity components (m/s)
u_τ	friction velocity (m/s)
u_i	velocity vector (m/s)
v	velocity of particle(m/s)
x_i	cartesian coordinate

1. Introduction

The COVID-19 pandemic has resulted in a significant loss of human life on a global scale. As on April 6th, 2023, the World Health Organization has reported a total of 762,201,169 confirmed cases of COVID-19 worldwide, with 6,893,190 reported deaths. Additionally, as of April 3rd, 2023, a total of 13,337,416,815 vaccine doses have been administered [1]. At the beginning it was predicted that the transmission of the virus occurred primarily through droplets expelled from coughing or sneezing, and that social distancing measures could be effective in interrupting the chain of infection, however, recent studies have revealed that the virus can, in fact, be transmitted through the air [2, 3]. The surges of COVID-19 cases have placed an immense strain on hospital systems, resulting in a negative impact on both healthcare and public health infrastructures. Due to limited capacity, medical facilities have been reserving their resources for patients with critical COVID-19 cases. Unfortunately, this has led to an elevated risk of transmission of the virus to non-SARS-CoV-2 patients and healthcare workers, ultimately increasing the probability of cross-contamination in these settings. To prevent and control infectious diseases, it is crucial to study the spread of contamination in intensive care units. Therefore, examining and understanding the patterns of contamination transmission in these settings is of utmost importance [4, 5].

To address the shortage of medical facilities, temporary hospitals have been constructed to provide centralized treatment for patients suffering from acute respiratory syndromes. The hospital spaces designated for treating patients with respiratory syndromes require special air conditioning systems with exhausts that can effectively remove harmful air particles emitted by the

patients [6]. Pathogens have diameters not exceeding 100 nanometers and move in response to air particles, making it difficult to analyze their movement paths. Many studies have shown to address this problem, , exploring various methods such as computational fluid dynamics simulations and experimental techniques. For instance, the authors discovered that the through the use of a suction fan in an isolation room, lifetime of airborne particles can be considerably reduced as a result of a lower local mean age of air [7]. In [8], the authors have presented a model that predicts airborne virus transmission in indoor areas. This model analyzed the impact of two key factors, namely the amount of social distancing and the efficacy of ventilation, by integrating them into the Wells-Riley model. In [9], the researchers have performed a study wherein they presented that even after a patient in the recovery stage of COVID left an ICU room, air samples taken from the same room still tested positive for COVID several days later. In addition, the authors of [9] emphasized the importance of increasing the frequency of indoor air disinfection based on their findings. Similarly, another study was conducted to examine the ventilation system of a COVID-19 isolation unit [10]. The results revealed that the virus had the ability to travel considerable distances through the central ventilation system. In [11], the authors have investigated an approach that analyze transmission of saliva particles arising from a human cough. This study highlights the significant influence of wind speed in an open space environment on the distance traveled by airborne disease-carrier droplets when a person coughs.

Many authors have used computational fluid dynamics (CFD)-based techniques to investigate the evolution of particle distribution within a hospital room. By utilizing the CFD solution of nonlinear Navier-Stokes equations, it is now possible to simulate highly complex fluid flows under various conditions and in different regions with great accuracy. For example, in [12, 4, 13, 14], the authors have used CFD. In [4], The authors employed the CFD method to investigate the evolution of particle distribution considering a single-bed hospital room. The study demonstrated how infections can spread and identified the paths of contamination. The authors concluded that increasing the air change rates (ACRs) leads to a more rapid elimination of airborne infections. Moreover, they emphasized that the distance to the outlet is a crucial factor in controlling infections. In [13], the authors have used CFD with $SSTk-\epsilon$ model to study the flow field in an isolation ward while air conditioning system and sanitizing machine are running. Similarly, in [12], a CFD model was presented by the authors to identify the ideal position for virus sensors. Their research revealed that the most suitable location for a sensor is at the center of the ceiling, and the accuracy of contaminant detection can be improved through a highly sensitive sensor and increasing the discharge time. The study based on CFD method assesses an emergency department's layout and airflow to identify potential risk areas for staff and patients [14]. Based on their findings, the researchers provide recommendations to improve the design and reduce the workload on hospitals. This would enable hospitals to operate at full capacity without compromising employee safety and disease transmission risks. The study in [15], uses CFD simulation to evaluate the ventilation system of an emergency department at a university hospital. The findings identify three critical areas that are more susceptible to viral transmission and provide recommendations for improving the placement of inlets and outlets, separating areas, and designing spaces and corridors. These changes can help prevent the spread of SARS-CoV-2 and other viruses within the hospital. In [16], the study investigates the impact of natural ventilation on the transmission of COVID-19 between patient rooms and adjacent areas. The study uses mechanical modeling and CFD simulation to analyze the effect of natural ventilation on virus transmission. Results show that positioning air inlet/outlets at the top or bottom of the room and maximizing natural air velocity reduces COVID-19 contamination dissemination. This study provides important insights for designing and implementing effective ventilation systems

to prevent the spread of COVID-19 in indoor spaces. The research in [17], provided valuable insights into the influence of weather conditions on the transmission and viability of airborne virus particles. The study developed new theoretical correlations for the unsteady evaporation of coronavirus-contaminated saliva droplets and implemented them in a computational fluid dynamics solver to explore the effects of weather factors on airborne virus transmission. The findings revealed that weather conditions, including relative humidity, temperature, and wind speed, play a significant role in the survival and transport of airborne virus particles, with implications for potential pandemic waves during different seasons. Furthermore, recent research by [18] sheds light on the impact of air ventilation systems on airborne virus transmission (AVT) in confined spaces. This study investigated the influence of ventilation designs on AVT in elevators, serving as a prototypical example of a confined space. Through computational fluid dynamics, the study examined the effects of different flow scenarios involving the position and operation of inlets and outlets in the elevator, as well as the performance of an air purifier for reducing AVT. The findings emphasize the significance of carefully considering the placement and design of air purifiers and ventilation systems in confined spaces to effectively manage droplet dispersion and mitigate AVT risks.

This paper provides the airflow patterns, particle transport and contaminant dispersion in isolation unit at Saniat Rmel Hospital in Tetouan Morocco, considering the effects of inlet air velocity and the combination of HAVC-sanitizer machines on the transport of particles that are suspended in the room. To achieve these objectives, we combine the use of Eulerian approach for simulation of the airflow continous phase and Lagrangian approach for discrete pahse to analyze the particle transport. Numerical simulation of turbulent flows presents inherent complexity, involving intricate motion occurring across various scales. To address this complexity, we employed the Reynolds-averaged Navier–Stokes equations. The CFD analysis shows that higher inlet velocity results in faster transport of particles and shorter travel times from air conditioner to exhaust port. The combination of air-conditioner and sanitizer systems is an efficient measure for controlling the spread of airborne particles and reducing the dispersion of the SARS-Cov-2 virus. These findings provide crucial insights for optimizing ventilation systems in hospital isolation rooms to mitigate the spread of viruses.

2. Methodology

To simulate the airflow and particle transport in the hospital isolation unit, we used a computational fluid dynamics (CFD) approach. CFD is a numerical method used to solve the governing equations that describe fluid flow [19, 20, 21, 22] and the behavior of particles suspended in the fluid. In this study, we used the finite element method (FEM) to discretize the governing equations and solve them numerically. The governing equations used in the simulation include continuity, momentum, turbulence model, energy, transport of concentrated species, and particle tracing for fluid flow. Continuity describes the conservation of mass in the fluid, while momentum describes the conservation of momentum. Energy describes the conservation of energy in the fluid. Transport of concentrated species describes the transport of a particular substance in the fluid, such as the sanitizer used in the isolation unit. Particle tracing for fluid flow describes the movement of particles suspended in the fluid.

To solve these governing equations, we used quadratic schemes with the Boussinesq approach [23], which allows us to account for the effects of turbulence on the fluid and particle behavior. Additionally, we carried out both steady-state and unsteady-state simulations to capture the be-

havior of particles over time. In the following sections, we will provide the specific equations used for each governing equation, as well as the numerical methods used to solve them.

The realizable $k-\epsilon$ turbulence model is used in this research with COMSOL Multiphysics code [24], which includes the two equations for the turbulent kinetic energy and its dissipation rate. This allows for more accurate modeling of the turbulence structure and behavior in complex flows.

2.1. Eulerian model (Continuous phase)

2.1.1. Governing equation and turbulence model

For an incompressible steady-state and Newtonian fluid, the Navier-Stokes and turbulence model equations can be written in the following form:

$$\frac{\partial \bar{u}_i}{\partial x_i} = 0 \tag{1}$$

$$\rho \frac{\partial \overline{u_i}}{\partial x_i} + \rho \overline{u_j} \frac{\partial \overline{u_i}}{\partial x_j} = -\frac{\partial \bar{p}}{\partial x_i} + \frac{\partial}{\partial x_j}\left(\mu\left(\frac{\partial \overline{u_i}}{\partial x_j} + \frac{\partial \overline{u_j}}{\partial x_j}\right) - \overline{\rho u_i' u_j'}\right) + \bar{f} \tag{2}$$

In this equation, $\bar{u}$ and p represent the mean flow velocity and pressure, respectively, while ρ denoting the fluid density. The variable f is used to describe additional forces, such as gravity, and μ represents the dynamic viscosity of the fluid. $-\overline{\rho u_i' u_j'}$ means the Reynolds stress term, which presents the fluctuating velocities in turbulent shear flows.

$$\tau_{ij} = -\overline{\rho u_i u_j'} = \mu_t\left(\frac{\partial \bar{u}_i}{\partial x_j} + \frac{\partial \overline{u_j}}{\partial x_i}\right) - \frac{2}{3}\rho k \delta_{ij} \tag{3}$$

where is the δ_{ij} Kronecker term.

$$\rho \overline{u_i} \frac{\partial k}{\partial x_j} = \frac{\partial}{\partial x_i}\left[\left(\mu + \frac{\mu_t}{\sigma_k}\right)\frac{\partial k}{\partial x_i}\right] + P_k - \rho\varepsilon \tag{4}$$

$$\rho \overline{u_i} \frac{\partial \varepsilon}{\partial x_j} = \frac{\partial}{\partial x_i}\left[\left(\mu + \frac{\mu_t}{\sigma_\varepsilon}\right)\frac{\partial \varepsilon}{\partial x_i}\right] + \sqrt{2} C_{s_1} S_{ij} \varepsilon - C_{s2} \rho \frac{\varepsilon^2}{k + \sqrt{v\varepsilon}} \tag{5}$$

with the turbulent viscosity presented by:

$$\mu_t = \rho C_\mu \frac{k^2}{\varepsilon}$$

where C_μ is defined by:

$$C_\mu = \frac{1}{A_0 + A_s \frac{kU^*}{\varepsilon}} \tag{6}$$

$$U^* = \sqrt{S_{ij} S_{ij} + \Omega_{ij} \Omega_{ij}} \tag{7}$$

$$\Omega_{ij} = \overline{\Omega_{ij}} - \varepsilon_{ijk}\omega_k - 2\varepsilon_{ijk}\omega_k \tag{8}$$

with $\overline{\Omega_{ij}}$ means the average rate of rotation tensor and ω_k is the angular velocity. A_0 and A_s are two constants and determined as:

$$A_0 = 4, A_s = \sqrt{6}\cos\varphi \tag{9}$$

$$\phi = \frac{1}{3}\arccos(\min(\max(\sqrt{6}W, 1), 1)) \tag{10}$$

$$W = \frac{S_{ij}S_{jk}S_k}{S^2} \tag{11}$$

C_{s1} is defined as:

$$C_{s1} = \max\left(\frac{\eta}{5+\eta}, 0.43\right) \tag{12}$$

$$\eta = S\left(\frac{k}{\varepsilon}\right) \tag{13}$$

The closure parameters of the realizable k − ε turbulence model were defined by [25] as:

$$C_{s2} = 1.9, \sigma_k = 1.0, \sigma_s = 1.2$$

2.1.2. Heat transfer equation

The current study utilizes the Heat Transfer in Fluids COMSOL interface in steady-state case to solve 15 as reported in [26].

$$\rho C_p u.\nabla T + \nabla \cdot q = Q \tag{14}$$

$$q = -k\nabla T \tag{15}$$

with ρ is the fluid density, C_p is the fluid heat capacity at constant pressure, k presents the fluid thermal conductivity, u is the fluid velocity field, and Q is the heat source.

2.1.3. Non-isothermal Multiphysics

Non-isothermal flow coupling in COMSOL refers to the simultaneous solution of the Navier-Stokes equations for fluid flow and the heat transfer equation for the temperature distribution within the fluid. This approach takes into account the fact that the temperature distribution within a fluid can affect the fluid flow pattern and vice versa. The Navier-Stokes equations describe the motion of fluid in response to pressure and viscous forces, while the heat transfer equation governs the transport of thermal energy within the fluid. The non-isothermal flow coupling feature in COMSOL is used in our calculation when the effect of turbulent fluid flow on temperature distribution.

$$-n.q = \rho C_p u_\tau \frac{T_w - T}{T^+} \tag{16}$$

where, u_τ is the friction velocity, T_w presents the wall temperature, $T^+$is the dimensionless temperature.

2.1.4. Transport of Concentrated Species

Moreover, the transport of concentrated species was solved to describe the mass fraction of water species from the sanitizer machine. The mathematical formulation of the equations that govern the transport of these species in fluid flows is as follows:

$$\rho(u.\nabla)\omega_i = -\nabla \cdot j_i + R_i \tag{17}$$

where R_i is the source term of species, ω_i is the mass fraction of air and water species, j_i is the diffusive mass flux of species i, and can be presented as:

$$j_i = -\left(\rho D_{i,m} + \frac{\mu_t}{S_{c_i}}\right)\nabla\omega_i - D_t^T\frac{\nabla T}{T} \tag{18}$$

where S_{c_t} presents the turbulent Schmidt number, and D_t^T is the turbulence thermal diffusion coefficient.

2.2. Lagrangian model (Discrete phase)

2.2.1. Particle tracing for fluid flow equation

The particle tracing for fluid flow (PTM) is employed for a discrete phase to investigate the trajectory of air-conditioner and sanitizer machine particles. Based on Newton's second law and considering the influence of drag force, gravity, and buoyancy, the Lagrangian model simulates the trajectory of each particle is tracked for an unsteady state process [27]. The trajectories of particles are computed by utilizing the aforementioned equations in conjunction with the fluid motion equations, including mass, momentum, and energy.

$$\frac{d\left(m_p v\right)}{dt} = F_t \tag{19}$$

$$F_t = F_g + F_D + F_a \tag{20}$$

$$F_g = m_p g\frac{\rho_p - \rho}{\rho_p} \tag{21}$$

The dominant force is the drag force, which obeys the Stokes drag law:

$$F_D = \frac{1}{\tau_p}m_p(u - v) \tag{22}$$

$$\tau_p = \frac{\rho_p d_p^2 C_c}{18\mu} \tag{23}$$

m_p is the mass of the particle, v is the velocity of the particle, u is the fluid velocity, τ_p is the particle velocity response time, ρ_p is the particle density, g is the acceleration of gravity, C_c presents the Cunningham correction factor, and F_a is any other additional external forces [27], and which can be neglected in the simulation.

The random walk model (DRW) is employed to describe the dispersion of particle fluid induced by turbulence. The model accounts for the instantaneous turbulent velocity fluctuations u_i', which are superimposed on the local air velocity [28, 27].

$$u_i' = \overline{u_i} + \zeta\sqrt{\frac{2k}{3}} \tag{24}$$

where k presents the turbulent kinetic energy, and ζ is a vector of uncorrelated Gaussian random numbers with unit variance.

Table 1: Dimensions of hospital isolation Unit CAD model

No	Surface Name	Length (m) x-direction	Width (m) y-direction	Height (m) z-direction
1	Unit	3.5 m	3.0 m	2.5 m
2	HAVC	1.1 m	0.8 m	0.3 m
3	Sanitizer machine	0.8 m	0.16 m	0.2 m
4	Exhaust port	0.49 m	0.5 m	0.12 m
5	Bed	2.13 m	1.2 m	1.05 m

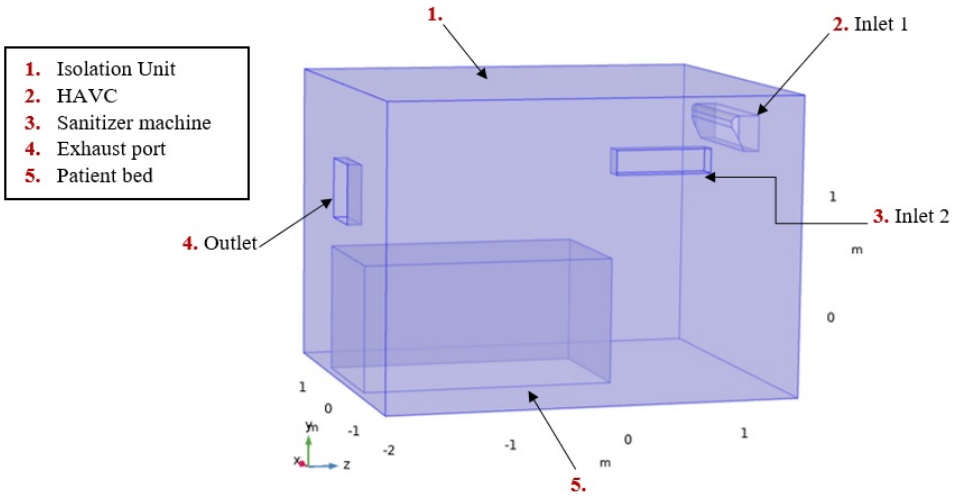

Figure 1: Configuration of a hospital isolation unit.

3. Hospital Unit Design

The hospital isolation unit used in this study consisted of a patient bed, a HAVC system, a sanitizer machine, and an exhaust port. The HAVC system was responsible for regulating the temperature and humidity of the air inside the room, while the sanitizer machine was used to release a fine mist of sanitizer particles into the air to kill any COVID-19 virus present.

A geometric model is created for the hospital isolation unit based on its real configuration. Using COMSOL Multiphysics, the CAD model of the hospital isolation unit, including the patient bed, heat air ventilation conditioning (HAVC) system, sanitizer machine, and exhaust port are built. To reduce computational costs, the patient's geometry is omitted, and only the patient's bed is included in the model. The unit features an HVAC system located opposite the bed, a sanitizer on one side, and an exhaust port outlet on the other side of the bed. Figure 1 provides a schematic representation of the isolation unit. The CAD model dimensions are summarized in Table 1 below. In this study, the dimensions of the sanitizer machine were fixed at (0.8m x 0.16m x 0.2m) for the numerical simulation. As a result, the proposed methodology can be readily applied to different computational physical models in the hospital unit.

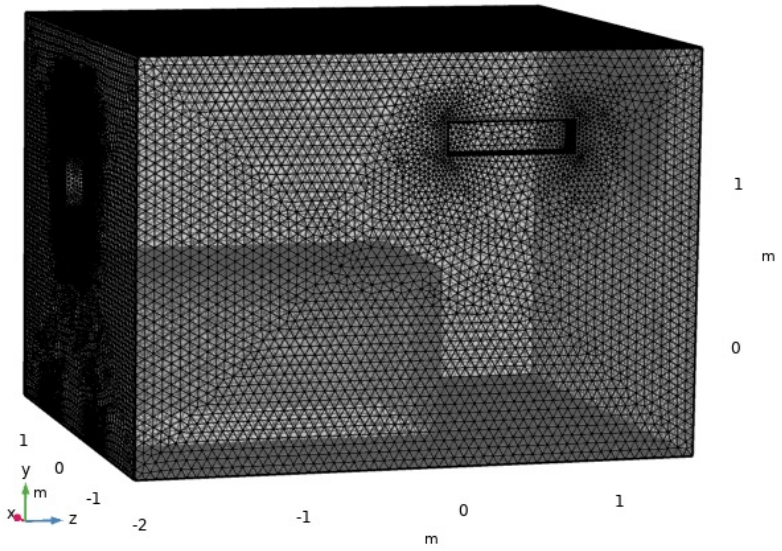

Figure 2: Mesh configuration of the isolation unit

4. Mesh and boundary condition

4.1. Mesh configuration and solver setup

The main isolation unit in the model has meshed using tetrahedral shapes in a 3D structure. To improve the accuracy of the numerical results, a finer mesh was employed in critical regions, such as near the inlet, outlet, and around the patient's bed. The mesh was composed of a total of 2265950 elements. Figure 2 illustrates the mesh configuration of the main isolation unit, which was created using hexahedral and tetrahedral elements for the patient bed, HAVC system, exhaust port, and sanitizer machine. The hexahedral mesh was used to construct complex regions, while the tetrahedral mesh was used for the remaining regions of the computational volumes.

For the 3D simulation, a commercial software package COMSOL Multiphysics was employed to solve the governing equations of continuity, momentum, and turbulence. In addition, the model incorporated the equations for heat transfer and transport of concentrated species. The particle tracing module was utilized for fluid flow analysis. The Navier-Stokes equations were discretized using the FEM to solve the CFD equations that include the conservation of mass, momentum, energy, transport of species, and particle trajectory. The turbulence variables, heat transfer, and transport of species were solved separately from momentum and pressure using a segregated solver. The particles were tracked using the Lagrangian approach, throughout this process, the continuous flow solution was maintained constant. The simulations were performed on a high-performance computing system, and the convergence criteria were set at a tolerance of 10^{-6} for temperature and 10^{-5} for all rest of the equations.

4.2. Boundary conditions

Various boundary conditions were used in the simulation to accurately represent the physical conditions inside the isolation unit. Given the significance of combining sanitizer-air conditioning to minimize virus diffusion, the inlet conditions for the air cold conditioning of the isolation

Table 2: Summary of boundary conditions

Continuous Phase: Eulerian (Turbulence flow Realizable $k-\epsilon$ Heat Transfer in Fluid Transport of concentrated species)	Inlet 1 (air-conditioner) Inlet 2 (Sanitizer machine) Outlet (Exhaust port) Wall	Air velocity inlet, different velocity= 3m/s; 4m/s; 5m/s Temperature= 21°C Turbulent intensity= 5%; Turbulent length scale= 0.01m. Pressure (Normal flow) = 0 Pa; Disappear. All remaining walls (Unit +Bed Patient): No slip-conditions; Thermal insulation
Discrete Phase: Lagrangian (Particle tracing for fluid flow)	Diameter (μ_m) Particle number Time step (s) of the simulation	D=0.5 N=1000 range (0,0.1,20)

unit were set at different values of the velocity of 3 m/s, 4m/s, and 5m/s, respectively, with an inlet temperature of 21°C. In addition to U=1.5m/s and T=35°C for the inlet of the sanitizer machine. The non-slip condition was applied to all surfaces, including walls and the patient bed. Additionally, turbulent intensity and length scale of 5% and 10%, respectively, were set as the inlet boundary conditions. At the outlets, a pressure outlet and "disappear" boundary condition were employed. The summary of all the boundary conditions is presented in Table 2.

5. Model Validation

Validating a simulation model is a crucial step in the simulation process, involving a comparison of the model's results with either experimental data or previously published findings, to ensure that the model accurately represents the physical system under investigation. Therefore, Figure 4 shows the validation of the current numerical model and methodology of the fluid flow velocity of the hospital isolation room geometry by comparing published experimental and numerical works [29, 30] from the various positions within the designed room (see Figure 3). The level of agreement between the model and published data can be observed in Figure 4, demonstrating the high quality of the model's validation.

6. Mesh independence study

The present model was assessed using four distinct mesh sizes, thereby achieving the maximum computational capacity of the system. The mesh sizes adopted in the study are presented in the Table 4 as follows: Figure 5 depicts the results of a mesh independence study, showing the effect of varying mesh sizes on the accuracy of simulation results. Four different mesh sizes were tested, ranging from an extra coarser mesh to a finer mesh. The x-axis shows the cut-line length, while the y-axis displays the value of the air velocity simulation results. Each line on the

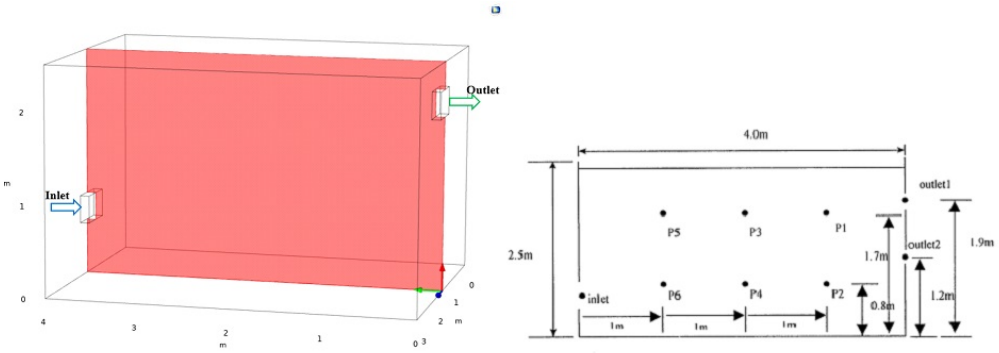

Figure 3: Computational domain used for model validation (left), and positions of measurement locations within the test chamber (right)

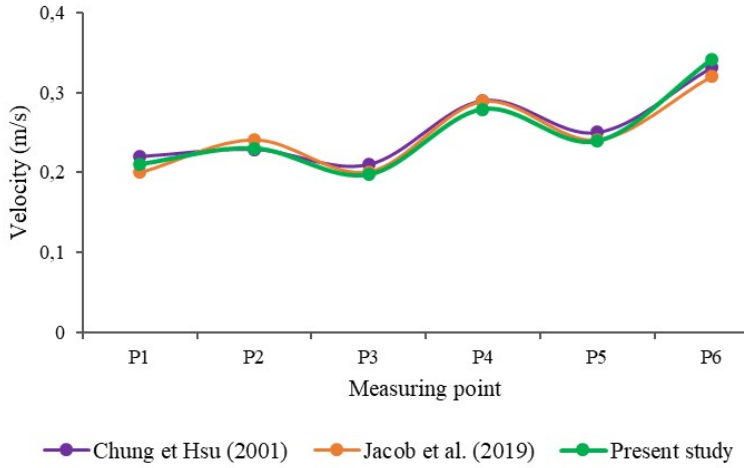

Figure 4: Velocity distribution at different positions within the test chamber [29], where an inlet velocity of 1.36 m/s is assumed.

Position	Velocity (m/s) (current study)	Velocity(m/s) (Chung et Hsu (2001))	Error
P1	0.21	0.22	0.04
P2	0.23	0.23	0
P3	0.20	0.21	0.05
P4	0.28	0.29	0.03
P5	0.24	0.25	0.04
P6	0.34	0.33	0.03

Table 3: Comparison of velocity (m/s)

Table 4: Characteristics of the mesh for V_{air}=4m/s

	Domain elements	Boundary elements	Edge elements	Mean velocity (m/s)
Mesh 1: Extra coarse	281678	17774	1089	1.1453
Mesh 2: Coarse	868075	36710	1635	1.1434
Mesh 3: Normal	1752243	70390	2554	1.1432
Mesh 4: Finer	2265950	83572	2622	1.1432

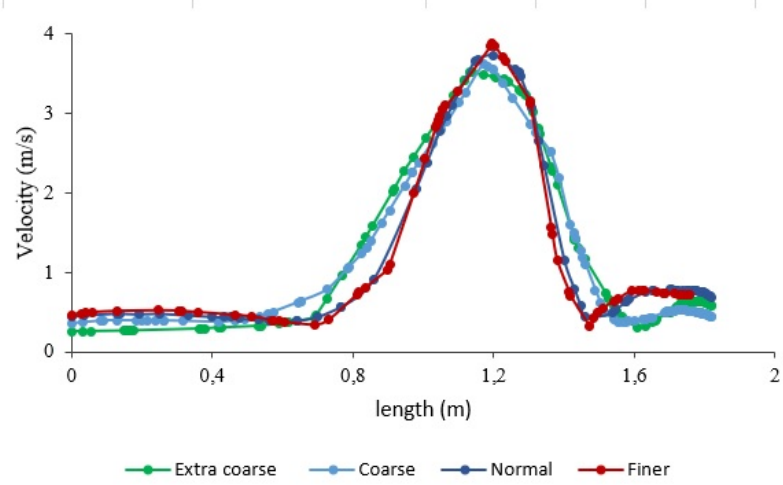

Figure 5: Grid independence study: Comparison of velocity magnitude distribution at cut-line for different mesh studies: case of V_{air}=4m/s.

graph represents the results obtained using a different mesh size. The figure demonstrates that the results are relatively consistent across all mesh sizes, indicating that the simulation is mesh independent beyond the normal mesh. Hence, this mesh is used for the following computation since the results are not significantly affected by the choice of the mesh size.

7. Results and discussions

In the context of our proposed airflow design methodology for hospital isolation units, the use of sanitizers serves as a critical adjunct to the HVAC system in reducing the potential transmission of respiratory pathogens, including SARS-CoV-2. An aerosolized disinfectant, delivered through an aerosol sanitizer delivery system is designed to complement the HVAC efforts by targeting the disinfection of indoor air and surfaces within the isolation room. This system disperses the sanitizer in the form of fine droplets or particles into the air of the isolation room, effectively neutralizing airborne pathogens. The timing of sanitizer application is meticulously coordinated

with the ventilation cycle or during periods when the room is unoccupied to prevent potential exposure to healthcare personnel or patients.

The theoretical framework developed in this study presents a promising approach to airflow design in hospital isolation units for reducing the potential transmission of SARS-CoV-2 and other respiratory pathogens. To ensure the practical applicability and reliability of the structure, robust validation is essential. In the Section 5, we have demonstrated the validation of our numerical model and methodology for fluid flow velocity within the hospital isolation room geometry by comparing our results with published experimental and numerical data [29, 30]. The level of agreement observed between our model and the published data provides confidence in the accuracy of our simulation approach.

The results of the CFD simulation inside a hospital isolation unit will be presented and explained in details below.

7.1. Velocity

Figure 6 presents the velocity distribution in slices, demonstrating that the blue-colored conditioned air is distributed throughout the isolation room. The velocity magnitude is quite low, measuring 0.08 m/s, and exhibits minimal variations. The velocity magnitude in Figure 7 was evaluated at different slice positions x=0, z=0.35, and z=-0.9 in the room, with varying air velocities from 3m/s to 5m/s. It can be observed that Case (a) has a relatively low-velocity magnitude throughout the room, with a maximum velocity of around 5.18 m/s. This could be an issue if the room has a high occupancy or if there are concerns about the spread of airborne particles[6]. The low-velocity magnitude near the patient bed and in the breathing zone is also concerning (planes x=0 and z=-0.9), as it suggests that the air may not be effectively removing airborne particles from those areas. In Case (b), the velocity magnitude is higher than in Case (a), with a maximum velocity of around 6.52 m/s. However, the velocity magnitude near the patient bed is still relatively low, indicating that additional measures may be necessary to ensure the effective removal of airborne particles from that area. Case (c) has the highest velocity magnitude, with a maximum velocity of around 7.84 m/s. This improvement over Cases (a) and (b) indicates that the air conditioning system is more effective at removing airborne particles around the patient bed (planes x=0 and z=-0.9), this could enhance their ability to propagate over longer distances and penetrate deeper into the room. The higher velocity magnitude near the air conditioning outlet in all cases suggests that the system is generating a stronger airflow pattern that could help to control the spread of airborne particles. The airflow patterns in an isolation unit were assessed using streamline velocity visualization in Figure 8. Case (a) had a somewhat turbulent airflow pattern with irregular movements, potentially hindering airborne particle removal. The patient's bed area had stagnant airflow. In Case (b), the airflow pattern was more regular and stronger, with some improvement in patient bed area airflow. Case (c) had highly turbulent airflow, showing that the air conditioning system and sanitizer machine were generating an effective and controlled airflow pattern, leading to highly effective airborne particle removal near the patient bed. The elevated velocity suggests that fluid particles, potentially including virus particles, exhibit increased mobility, facilitating the potential for longer-distance travel within the room. This underscores the significance of the air conditioner's placement and direction in influencing the transport dynamics of fluid particles. This broad interpretation is derived from the analysis of the velocity field.

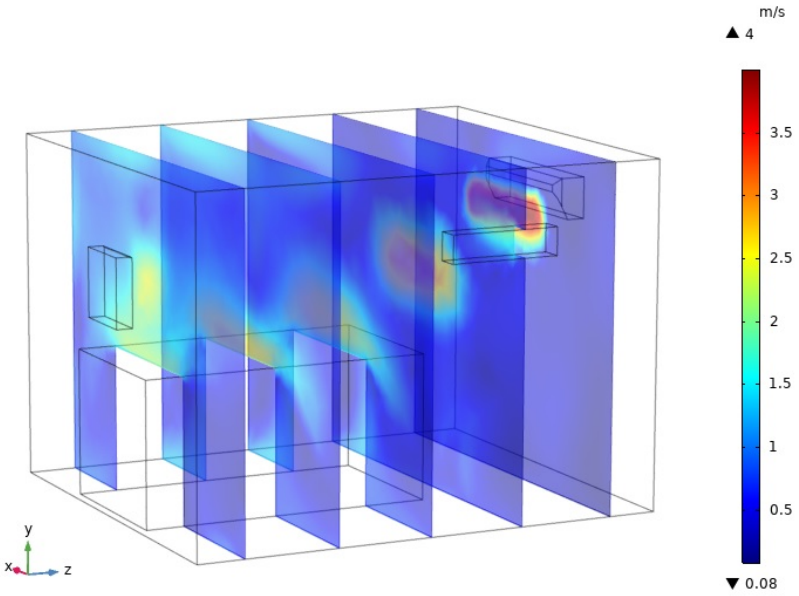

Figure 6: Velocity magnitude distribution in hospital isolation unit: Slices illustrating airflow patterns for V_{air}=4m/s.

7.2. Temperature

The temperature was also an important factor in the simulation (see Figures 9 and 10), as the cold air from the air conditioning unit at 21°C mixed with the hot sanitizer at 35°C. Figure 9 presents the differences in temperature distribution between the two slices (x=0 and z=0.35) and the impact of the air-conditioner and sanitizer machine on the thermal environment of the hospital isolation room. The simulation results showed that the temperature distribution in the room was uneven, with higher temperatures near the sanitizer and lower temperatures near the air conditioning unit. This suggests that the combined approach may be most effective when the sanitizer is positioned near the patient's bed, where the virus is most likely to be present. The streamline temperature visualization in Figure 10illustrates that cooler temperatures, represented by yellow, are present near the air-conditioning system with temperatures around 21°C. As the air flows into the room, it begins to warm up, with temperatures reaching around 25°C in some areas. While warmer temperatures, represented by red, which comes from the right of the air conditioning are present near the sanitizer machine with temperatures around 35°C. The mixing of these temperatures creates a complex temperature distribution throughout the room, with some areas reaching temperatures as high as 30°C, while others remain cooler, with temperatures around 22°C. Thus, effective disinfection of the environment requires careful consideration of this temperature distribution.

Moreover, the observed temperature distribution within the hospital isolation room, as depicted in Figures 9 and 10, aligns with the findings presented in reference [18]. Our simulations revealed that the combination of cold air from the air conditioning unit (21°C) and hot sanitizer (35°C) results in an uneven temperature profile. Notably, higher temperatures are concentrated near the

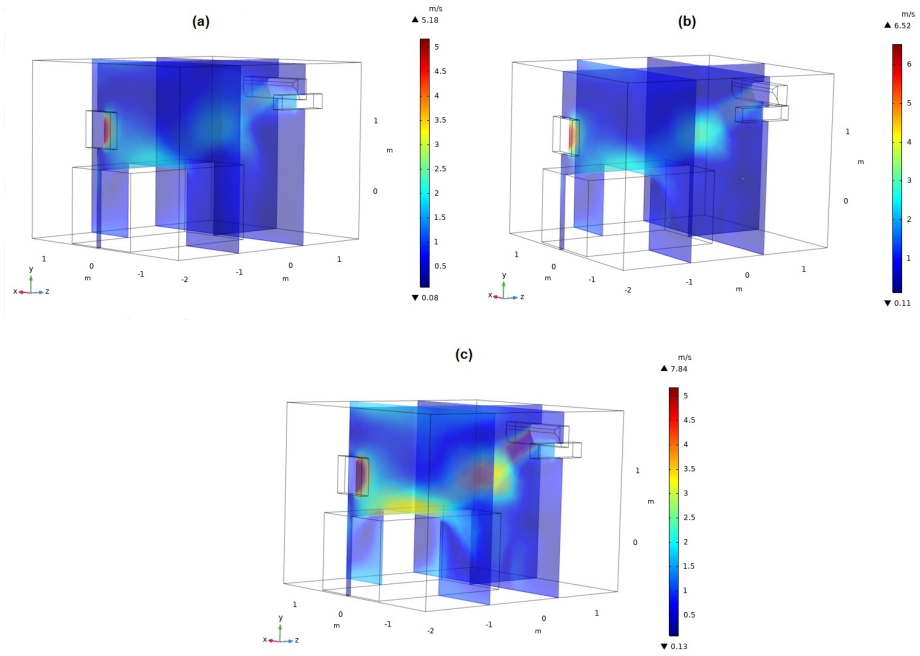

Figure 7: Velocity magnitude distribution, (a) V_{air}=3m/s, (b)V_{air}=4m/s, (c) V_{air}=5m/s for various positions of slices in the hospital isolation unit: x=0; z=-0.9; z=0.35.

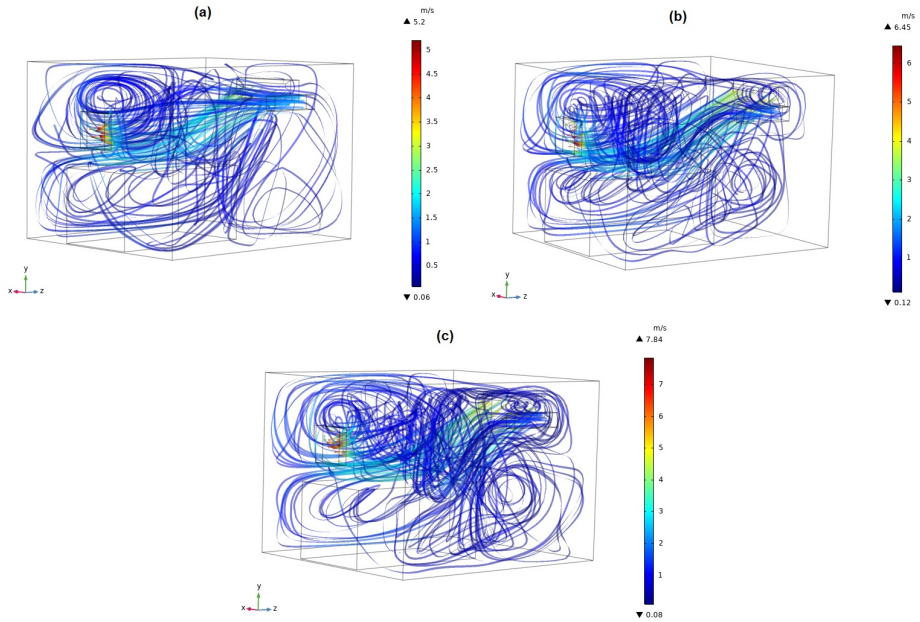

Figure 8: Presentation of velocity magnitude patterns in the hospital isolation unit for three cases of air-velocity: (a) V_{air}=3m/s, (b)V_{air}=4m/s, (c) V_{air}=5m/s

sanitizer, while lower temperatures prevail in proximity to the air conditioning unit. The significance of this distribution is illuminated by the insights from [17], where the authors demonstrate that elevated temperatures and low relative humidity contribute to increased evaporation rates of saliva-contaminated droplets. This phenomenon, quantified through three-dimensional CFD simulations, substantially reduces virus viability. Moreover, the study [17] underscores that even at elevated temperatures, the effectiveness of disinfection strategies is contingent on the relative humidity levels. These correlations emphasize the need for careful consideration of temperature and humidity dynamics in optimizing disinfection protocols within the isolation room, in accordance with the nuanced findings from our simulations and the referenced study [17].

7.3. Turbulent kinetic energy

This work discusses the use of turbulent kinetic energy (TKE) results to analyze fluid flow and transport in a hospital isolation unit under different cases of air-conditioning inlet velocity. Lower levels of TKE (Figure 11 (a) and (b)) may be associated with less turbulence and more stable flow, resulting in lower mixing and transport of particles or species, while higher levels of TKE (Figure 11 (c)) may indicate more intense turbulence and greater mixing and transport, but with an increased risk of flow instability and turbulence-related issues. The TKE results can provide valuable insights into the impact of turbulence on fluid flow and transport and can be used to optimize the design and operation of ventilation and filtration systems.

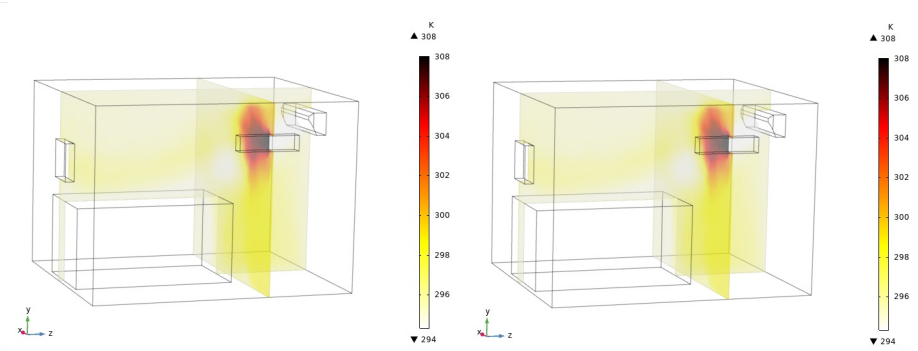

Figure 9: Temperature contour-plot in hospital isolation unit for V_{air}=4m/s: Cross-Sections of air-conditioner and sanitizer machine (Left); temperature (x-y) side view (right).

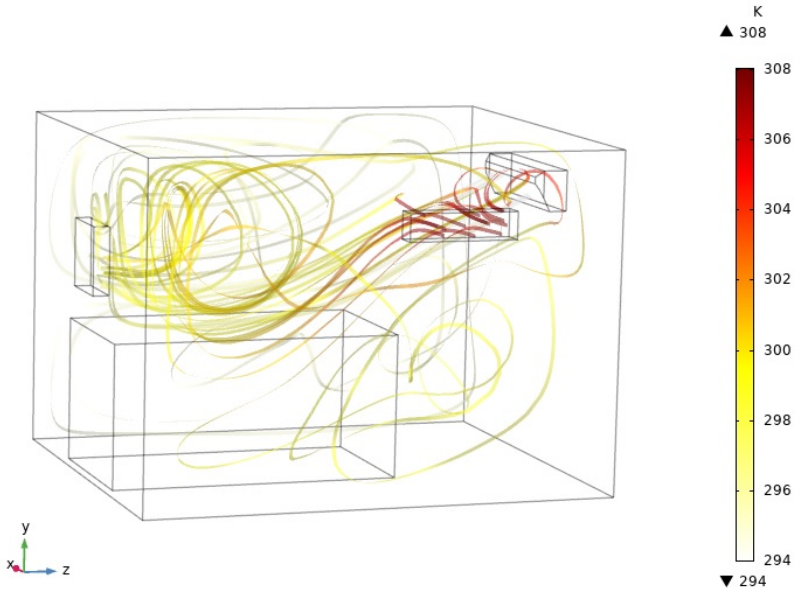

Figure 10: Patterns distribution in a hospital isolation unit with temperature in Kelvin for V_{air}=4m/s.

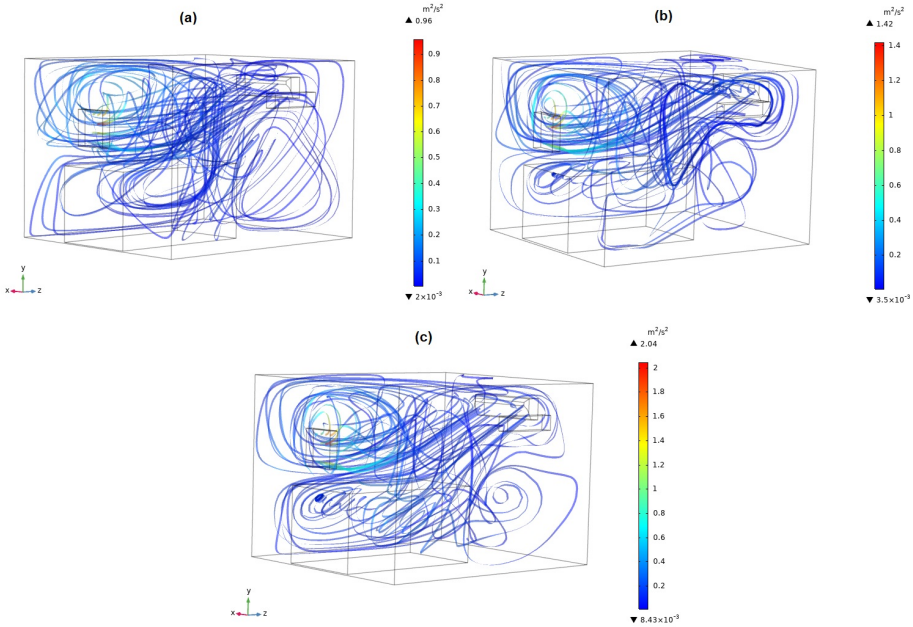

Figure 11: Patterns of turbulent kinetic energy (TKE) in a hospital isolation unit for three air-velocity cases: (a) V_{air}=3m/s, (b)V_{air}=4m/s, (c) V_{air}=5m/s

7.4. Transport of concentrated species

Figure 12 shows how the pathogen concentration changes in different areas of the unit as the inlet air velocity varies. It can be seen that the molar concentration of the virus decreases slightly as the inlet air velocity increases from 3m/s to 5m/s in the hospital isolation unit. This result can be useful in identifying areas of high pathogen concentration. Additionally, the simulation results may help in determining the optimal air change rate required to minimize the concentration of the pathogens and reduce the risk of transmission. On the other hand, the simulation showed that the concentration of sanitizer particles increased near the patient bed, where the virus is most likely to be present. This demonstrates that the proposed approach can effectively deliver sanitizer particles to the areas where they are most needed.

7.5. Particle tracing of fluid flow

Figure 13 demonstrated the particle trajectory simulation and showed that the particles from the air conditioning and sanitizer machine were able to travel throughout the room, with some particles returning to the sanitizer and air conditioning unit through the exhaust port. Particle trajectory analysis (see Figure 14) was conducted in three different cases to assess the impact of the velocity of the air-conditioning inlet on particle transport. In Case (a), with an inlet velocity of 3 m/s, particles take longer to reach the exhaust port due to the lower airflow resulting from the lower mixing of particles. Case (b), with an inlet velocity of 4 m/s, exhibits faster particle transport compared to Case (a), attributed to higher airflow and more particle mixing. In Case (c), with an inlet velocity of 5 m/s, the fastest particle transport is observed, which is attributed

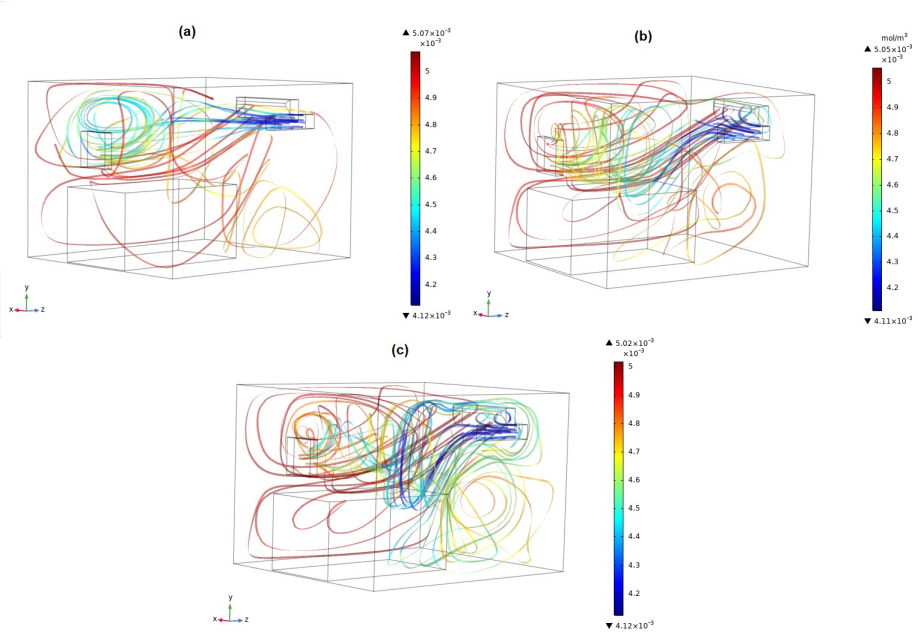

Figure 12: Patterns distribution in the hospital isolation unit with a molar concentration in mol/m^3 for three air-velocity cases: (a) V_{air}=3m/s, (b)V_{air}=4m/s, (c) V_{air}=5m/s

to the highest air flow and greater mixing of particles. The findings highlight the importance of airflow and particle mixing in particle transport and the need to optimize inlet velocity for the effective removal of airborne particles.

8. Conclusion

This investigation presents a comprehensive study of the airflow dynamics and contaminant dispersion in isolation unit at Saniat Rmel Hospital in Tetouan Morocco, by considering the combination of the HAVC-sanitizer machine and the effect of inlet air velocity on the results. A comprehensive CFD analysis was conducted by using the realizable $k-\epsilon$ turbulence model. The study shows that the inlet air velocity has a significant impact on the temperature distribution, velocity distribution, turbulent kinetic energy, and particle trajectories in the isolation unit. It demonstrated that a higher inlet velocity for the air-conditioner system results in higher velocity magnitudes throughout the room, and leads to fast transport of particles and shorter travel times from the air conditioner to the exhaust port. However, it is noteworthy that, as discussed in [6], the increased ventilation associated with higher inlet velocity can have some downsides. Additionally, [6] mentions that double airflow of HVAC considerably enhances the motion of turbulent air, resulting in the spread of contaminated air and airborne viruses over a larger space. This suggests that while increased ventilation is positive for smaller spaces like the isolation room, in larger spaces it can potentially spread viral particles throughout a larger area. Such results offer a crucial understanding of the dynamics of particles within the enclosed environment, emphasizing the significance of boundary conditions in regulating their dissemination. The sim-

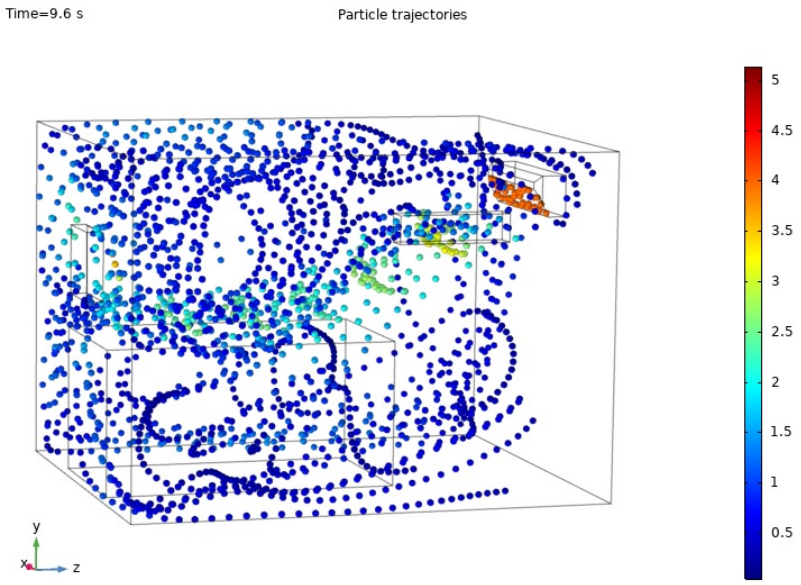

Figure 13: Particle tracing in a hospital isolation unit for V_{air}=4m/s: Illustrating airflow patterns and particle dispersion.

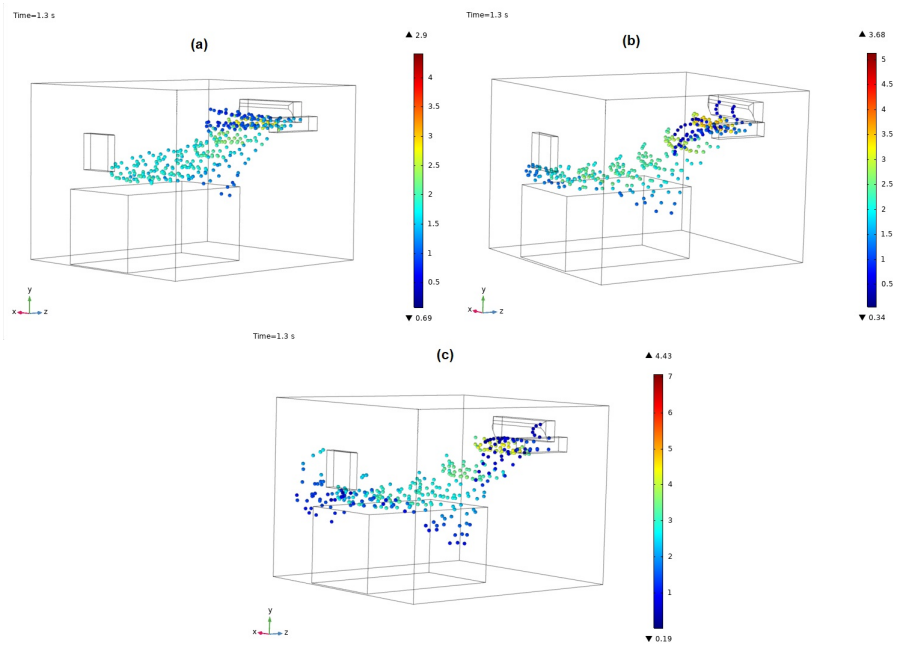

Figure 14: Particle tracing in a hospital isolation unit in t=1.3s for three air-velocity cases:(a) V_{air}=3m/s, (b)V_{air}=4m/s, (c) V_{air}=5m/s

ulation outcomes indicated that the combination of the air-conditioner and sanitizer systems and their emplacement optimization proves to be an efficient measure of controlling the spread of airborne particles and reducing the dispersion of the SARS-Cov-2 virus in the isolation unit.

Acknowledgements

The researchers would like to extend their appreciation to ENDESA for generously funding this research project, as well as to the Institute of Mathematical Sciences (ICMAT) for their valuable support and provision of necessary resources and facilities for conducting this study.

References

[1] W. H. Organization, Who coronavirus (covid-19) dashboard (2023).
URL https://covid19.who.int/

[2] E. Martínez-Espinosa, I. Carvajal-Mariscal, Virus-laden droplet nuclei in vortical structures associated with recirculation zones in indoor environments: A possible airborne transmission of sars-cov-2, Environmental Advances (2023) 100376.

[3] S. C. Moharir, S. C. Thota, A. Goel, B. Thakur, D. Tandel, S. M. Reddy, A. Vodapalli, G. S. Bhalla, D. Kumar, D. S. Naruka, et al., Detection of sars-cov-2 in the air in indian hospitals and houses of covid-19 patients, Journal of Aerosol Science 164 (2022) 106002.

[4] T. N. Verma, A. K. Sahu, S. L. Sinha, Numerical simulation of air pollution control in hospital, Air Pollution and Control (2018) 185–206.

[5] C. E. Madubueze, S. Dachollom, I. O. Onwubuya, Controlling the spread of covid-19: optimal control analysis, Computational and Mathematical methods in Medicine 2020 (2020).

[6] F. Mohamadi, A. Fazeli, A review on applications of cfd modeling in covid-19 pandemic, Archives of Computational Methods in Engineering 29 (6) (2022) 3567–3586.

[7] P. Yuen, R. Yam, R. Yung, K. Choy, Fast-track ventilation strategy to cater for pandemic patient isolation surges, Journal of Hospital Infection 81 (4) (2012) 246–250.

[8] C. Sun, Z. Zhai, The efficacy of social distance and ventilation effectiveness in preventing covid-19 transmission, Sustainable cities and society 62 (2020) 102390.

[9] T. Jin, J. Li, J. Yang, J. Li, F. Hong, H. Long, Q. Deng, Y. Qin, J. Jiang, X. Zhou, et al., Sars-cov-2 presented in the air of an intensive care unit (icu), Sustainable cities and society 65 (2021) 102446.

[10] K. Nissen, J. Krambrich, D. Akaberi, T. Hoffman, J. Ling, Å. Lundkvist, L. Svensson, E. Salaneck, Long-distance airborne dispersal of sars-cov-2 in covid-19 wards, Scientific reports 10 (1) (2020) 1–9.

[11] T. Dbouk, D. Drikakis, On coughing and airborne droplet transmission to humans, Physics of Fluids 32 (5) (2020).

[12] T. Zhang, Q. Y. Chen, C.-H. Lin, Optimal sensor placement for airborne contaminant detection in an aircraft cabin, HVAC&R Research 13 (5) (2007) 683–696.

[13] S. Bhattacharyya, K. Dey, A. R. Paul, R. Biswas, A novel cfd analysis to minimize the spread of covid-19 virus in hospital isolation room, Chaos, Solitons & Fractals 139 (2020) 110294.

[14] O. F. Alrebi, B. Obeidat, I. A. Abdallah, E. F. Darwish, A. Amhamed, Airflow dynamics in an emergency department: A cfd simulation study to analyse covid-19 dispersion, Alexandria Engineering Journal 61 (5) (2022) 3435–3445.

[15] B. Obeidat, O. F. Alrebei, I. A. Abdallah, E. F. Darwish, A. Amhamed, Cfd analyses: The effect of pressure suction and airflow velocity on coronavirus dispersal, Applied Sciences 11 (16) (2021) 7450.

[16] H. Hassanzadeh, S. Shahrigharahkoshan, et al., Covid-19 dissemination assessment through natural ventilation in hospital patient room by cfd analysis, Journal of Architectural Research and Education 3 (1) (2021) 1–13.

[17] T. Dbouk, D. Drikakis, Weather impact on airborne coronavirus survival, Physics of Fluids 32 (9) (2020).

[18] T. Dbouk, D. Drikakis, On airborne virus transmission in elevators and confined spaces, Physics of Fluids 33 (1) (2021).

[19] A. Narjisse, K. Abdellatif, Analysis of obstacle and soil roughness effects on the wind speed profile by using the finite element method, Procedia Engineering 181 (2017) 770–776.

[20] A. Narjisse, A. Khamlichi, Computational fluid dynamics simulation to predict the airflow and turbulence in a wind farm in open complex terrain, in: Proceedings, Vol. 63, MDPI, 2020, p. 33.

[21] A. Narjisse, K. Abdellatif, Assessment of rans turbulence closure models for predicting airflow in neutral abl over hilly terrain, International Review of Applied Sciences and Engineering 12 (3) (2021) 238–256.

[22] S. Anas, A. Narjisse, E. K. Abderrahman, Modelling of neutral-stratified atmospheric boundary layer with commercial cfd software for the horizontal homogeneity thermo-fluid problem, in: The 16th International Conference Interdisciplinarity in Engineering: Inter-Eng 2022 Conference Proceedings, Springer, 2022, pp. 649–659.
[23] J. Boussinesq, Essai sur la théorie des eaux courantes, Impr. nationale, 1877.
[24] C. Multiphysics, Introduction to comsol multiphysics®, COMSOL Multiphysics, Burlington, MA, accessed Feb 9 (2018) (1998) 32.
[25] T.-H. Shih, W. W. Liou, A. Shabbir, Z. Yang, J. Zhu, A new $k-\epsilon$ eddy viscosity model for high reynolds number turbulent flows, Computers Fluids 24 (3) (1995) 227–238. doi:https://doi.org/10.1016/0045-7930(94)00032-T.
[26] D. C. Wilcox, et al., Turbulence modeling for CFD, Vol. 2, DCW industries La Canada, CA, 1998.
[27] B. Zhao, C. Yang, X. Yang, S. Liu, Particle dispersion and deposition in ventilated rooms: Testing and evaluation of different eulerian and lagrangian models, Building and Environment 43 (4) (2008) 388–397.
[28] L. Tian, G. Ahmadi, Particle deposition in turbulent duct flows—comparisons of different model predictions, Journal of Aerosol Science 38 (4) (2007) 377–397.
[29] K.-C. Chung, S.-P. Hsu, Effect of ventilation pattern on room air and contaminant distribution, Building and Environment 36 (9) (2001) 989–998.
[30] S. Jacob, S. S. Yadav, B. S. Sikarwar, Design and simulation of isolation room for a hospital, in: Advances in Fluid and Thermal Engineering: Select Proceedings of FLAME 2018, Springer, 2019, pp. 75–93.